Hierarchically Structured Microfibers of "Single Stack" Perylene Bisimide and Quaterthiophene Nanowires

Roman Marty,[†] Ruth Szilluweit,[†] Antoni Sánchez-Ferrer,[‡] Sreenath Bolisetty,[‡] Jozef Adamcik,[‡] Raffaele Mezzenga,[‡] Eike-Christian Spitzner,[§] Martin Feifer,[§] Stephan N. Steinmann,[⊥] Clémence Corminboeuf,[⊥] and Holger Frauenrath[†,*]

[†]Institute of Materials, Laboratory of Macromolecular and Organic Materials, Ecole Polytechnique Fédérale de Lausanne (EPFL), EPFL — STI — IMX — LMOM, MXG 037, Station 12, 1015 Lausanne, Switzerland, [‡]Department of Health Sciences and Technology, ETH Zürich, 8092 Zürich, Switzerland, [§]Fakultät für Naturwissenschaften, Technische Universität Chemnitz, 09126 Chemnitz, Germany, and [⊥]Institute of Chemical Sciences and Engineering, Laboratory for Computational Molecular Design, Ecole Polytechnique Fédérale de Lausanne (EPFL), Lausanne, Switzerland. R.M. prepared the compounds, developed the solution-spinning of microfibers, and performed IR, VCD, UV—vis, and CD spectroscopy, as well as POM, polarized IR microscopy, and AFM imaging of microfibers. R.S. performed SEM imaging. E.C.S. and M.F. performed MUSIC mode AFM imaging. A.S.F. and R.M. performed and interpreted SAXS and WAXS experiments, while S.B. did SLS, and J.A. contributed AFM imaging. S.N.S. and C.C. performed molecular dynamics simulations and DFT calculations. All previous authors contributed to the preparation of the manuscript. H.F. had the idea, designed and directed the research, and wrote the manuscript. The authors declare no competing financial interests.

ABSTRACT Organic nanowires and microfibers are excellent model systems for charge transport in organic semiconductors under nanoscopic confinement and may be relevant for future nanoelectronic devices. For this purpose, however, the preparation of well-ordered organic nanowires with uniform lateral dimensions remains a challenge to achieve. Here, we used the self-assembly of oligopeptide-substituted perylene bisimides and quaterthiophenes to obtain well-ordered nanofibrils. The individual nano-

fibrils were investigated by spectroscopic and imaging methods, and the preparation of hierarchically structured microfibers of aligned nanofibrils allowed for a comprehensive structural characterization on all length scales with molecular level precision. Thus, we showed that the molecular chirality resulted in supramolecular helicity, which supposedly serves to suppress lateral aggregation. We also proved that, as a result, the individual nanofibrils comprised a single stack of the π-conjugated molecules at their core. Moreover, the conformational flexibility between the hydrogen-bonded oligopeptides and the π—π stacked chromophores gave rise to synergistically enhanced strong π—π interactions and hydrogen-bonding. The result is a remarkably tight π—π stacking inside the nanofibrils, irrespective of the electronic nature of the employed chromophores, which may render them suitable nanowire models to investigate one-dimensional charge transport along defined π—π stacks of p-type or n-type semiconductors.
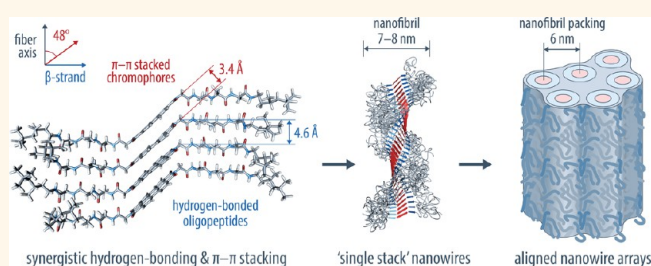
KEYWORDS: supramolecular self-assembly · "single stack" nanofibrils · hierarchically structured microfibers · organic nanowires · quaterthiophenes · perylene bisimides

Well-defined organic nanowires containing oriented π-conjugated segments and microfibers formed from aligned nanowire arrays are possible building blocks for chemical sensors,[1−3] photovoltaic devices,[4−6] as well as future nanoelectronic circuits.[7−9] They may, furthermore, provide suitable model systems for the investigation of charge generation and transport[10] under nanoscopic confinement.[11] As recently reviewed,[12] one-dimensional nanostructures of π-conjugated molecules have successfully been obtained by "top-down" approaches such as templating methods, electrospinning, or nanolithography. On the other hand, "bottom-up" approaches such as physical vapor deposition[12] and solution-phase approaches are considered to be a powerful strategy for the controlled organization of π-conjugated molecules into higher order objects. Thus, controlled anisotropic crystallization has abundantly been employed to obtain crystalline one-dimensional ribbons and rods comprising oriented stacks of

π-conjugated molecules from solution.[13−21] However, the preparation of well-ordered organic nanowires with uniform lateral dimensions formed from a defined number of π-conjugated cores per cross-section remains challenging. Well-defined nanofibrils have more recently been obtained by solution-phase self-assembly of tailored molecules,[22−25] including nanofibrils from trialkyloxyarylamide or oligopeptide-substituted π-conjugated molecules.[26,27] Microfibers comprising aligned nanofibril arrays were prepared by solvophobic bundle formation,[28] and control of microfiber diameters was achieved by solution spinning[29] or filament extrusion.[30,31] The capability of such microfibers to efficiently transport charge carriers is determined by a number of structural factors on different length scales, including the molecular structure of the chromophores, the supramolecular π−π interactions between them,[32] their aggregation into nanowires, and the packing of the latter into microfibers. It seems, therefore, beneficial to develop a pathway to guide the hierarchical self-organization of π-conjugated molecules irrespective of their electronic nature.[33] In this context, we recently found oligopeptide-substituted quaterthiophenes to give rise to nanowires that allowed us to observe photoinduced polaron generation and transport. Self-assembly of the π-conjugated cores into nanofibrils with excellent π−π overlap was achieved by using oligopeptide-polymer substituents to promote one-dimensional aggregation by β-sheet-like hydrogen-bonding, while supramolecular helicity and polymer attachment served to suppress lateral aggregation.[34]

Here, we report how supramolecular helicity combined with synergistically enhanced π−π stacking and hydrogen-bonding results in well-ordered nanofibrils from either the electron-poor perylene bisimide **1** or the electron-rich quaterthiophene **2**. The nanofibrils were shown to have uniform lateral dimensions, comprising single stacks of the π-conjugated chromophores at their core. Moreover, we processed the nanofibrils into well-defined hierarchically structured microfibers with detailed structural control on all length scales that we characterized with molecular level precision (Figure 1). Thus, the many centimeters long microfibers exhibited tailored diameters and an excellent internal alignment of the tightly packed nanofibrils. More importantly, the constituting molecules were proven to show a very tight π−π stacking, promoted by the strong hydrogen-bonding of the oligopeptide substituents in a hydrophobic environment and the inclusion of conformational flexibility in the molecular design. We, hence, demonstrate a versatile approach to prepare one-dimensional nano- and microstructures of π-conjugated molecules irrespective of their electronic nature, which is an important step toward complex organic nanoelectronic devices comprising p- and n-type semiconducting charge percolation paths.

RESULTS AND DISCUSSION

Spectroscopy of Aggregates in Solution. The oligopeptide-polymer modified perylene bisimide **1** and quaterthiophene **2** were synthesized analogous to published procedures.[34] Optically clear dispersions of **1** and **2** were obtained upon thorough thermal annealing in 1,1,2,2-tetrachloroethane (TCE), which provides a hydrophobic environment to induce strong hydrogen-bonding of the oligopeptides but is a good solvent for the attached poly(isobutylene) segments. The combination of infrared (IR), vibrational circular dichroism (VCD), UV−vis, and circular dichroism (CD) spectroscopy in solution proved that both **1** and **2** gave rise to very stable and well-defined hydrogen-bonded aggregates in organic solvents and, as a result, exhibited strongly π−π stacked chromophores in a helical arrangement. Thus, the presence of a single absorption band at 3290 cm^{-1} in the amide A region (ν_{N-H}) of the solution-phase IR spectra of **1** and **2**, a sharp band at around 1630 cm^{-1} in the amide I region ($\nu_{C=O}$), as well as the absence of the secondary amide I component at 1695 cm^{-1} were all consistent with the formation of strongly aggregated and well-ordered parallel β-sheet-like aggregates in both cases (Supplementary Figure S1). Furthermore, VCD showed a strong negative couplet for the amide C=O groups of **1** as well as a positive couplet for **2** in the amide I region (Figure 2a,b), proving that the amide C=O formed extended, resonance-coupled arrays in both cases. This was further confirmed by static light scattering (SLS) on solutions of **2** (Supplementary Figure S2) that revealed the presence of semiflexible fibrillar aggregates with a fractal exponent of about 5/3, indicative of excluded volume interactions.[35] Furthermore, UV−vis spectroscopy revealed that the main absorption bands of both perylene bisimide **1** (463 nm) and quaterthiophene **2** (371 nm) were significantly blue-shifted as compared to those of the molecularly dissolved species (Figure 2c,d; Supplementary Figures S3, S4). In the case of **1**, the remarkably strong blue-shift of the main absorption combined with the simultaneous appearance of bathochromically shifted absorption bands suggested the presence of strongly cofacially aggregated but both laterally and rotationally displaced perylene bisimide cores, resulting in strong spectral broadening due to H- and J-type bands.[36] By comparison, the blue-shifted spectrum of the quaterthiophene **2** also exhibited a barely visible red-shifted shoulder. This formation of spectroscopic H aggregates with an only weakly allowed HOMO−LUMO (highest occupied, lowest unoccupied molecular orbital) transition is indicative of predominantly rotationally and marginally laterally displaced arrangement of neighboring quaterthiophene chromophores.
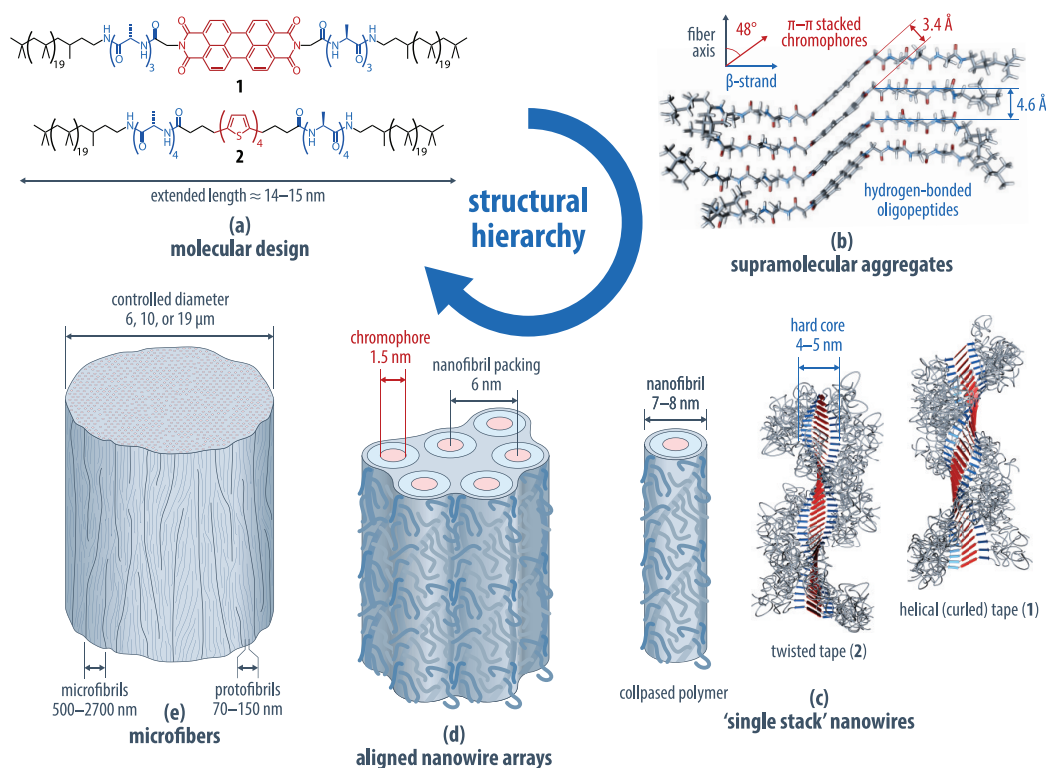
Figure 1. (a) Because of the molecular architecture of the difunctional, oligo(ʟ-alanine)-poly(isobutylene)-substituted perylene bisimide **1** and quaterthiophene **2**, the molecules (b) aggregated by synergistically enhanced β-sheet-like hydrogen-bonding (of the oligopeptide segments) and π–π stacking (of the central chromophores). (c) As a consequence of molecular chirality and polymer attachment, lateral aggregation is suppressed in solution, so that curled (helical) or twisted tapes are obtained that are formed from single stacks of the chromophores. (d,e) Hierarchically structured microfibers were prepared by solution spinning that comprise highly aligned arrays of the randomly close-packed nanofibrils, in which the attached polymer collapses to fill the tapes' helix grooves.

While the aggregates of **1** and **2** were so stable that they could not be thermally deaggregated in solution even upon heating to 373 K at low concentrations, titration of the solutions with a significant excess of trifluoroacetic acid (TFA) as a hydrogen-bond-breaking agent furnished molecularly disperse solutions of **1** and **2** that exhibited UV–vis absorptions at 537 and 404 nm, respectively. Moreover, solutions of both **1** and **2** exhibited strong CD activity with a positive Cotton effect for the highest wavelength absorption of **1** and a negative Cotton effect for **2**, while the molecularly disperse solutions obtained by deaggregation with TFA showed no CD activity at all. In combination, the spectroscopic findings provided unambiguous evidence that both **1** and **2** gave rise to extended one-dimensional aggregates with strongly π–π stacked chromophores in solution, with the laterally and rotationally displaced perylene bisimides of **1** in a *P*-helical (right-handed helical) environment, and the predominantly rotationally displaced quaterthiophenes of **2** in an *M*-helical (left-handed twisted) arrangement.[37−41]

Visualization of "Single Stack" Nanofibrils. AFM imaging of samples on mica substrates from thermally annealed TCE solutions revealed that perylene bisimide **1** (Figure 3a) gave rise to nanofibrils with lengths of

several micrometers, mostly uniform heights of about 4 nm, and defined apparent diameters of approximately 12 nm (subject to convolution with the AFM tip shape). Although the thermal annealing of the sample solutions only induced marginal differences in the IR, UV–vis, and CD spectra, it turned out to be the decisive factor to reproducibly obtain very long and uniform nanofibrils (Supplementary Figure S5). This does not prove that the nanofibrils are formed under thermodynamic as opposed to kinetic control, but the improved reproducibility may still be seen as an indication that the system is moving closer towards equilibrium. The tendency of the nanofibrils to laterally align on highly oriented pyrolytic graphite (HOPG) substrates (Supplementary Figure S6) allowed us to more accurately determine their true diameters to be 8.1 ± 1.4 nm. Moreover, the AFM images on mica substrates occasionally revealed segments with regular height corrugations mostly with a periodicity on the order of 80 nm, although segments with smaller periodicities of 20−30 nm were also observed. Phase images showed "diagonal" features consistent with the presence of right-handed helical or twisted tapes. Samples of quaterthiophene **2** on mica substrates essentially showed similarly well-defined nanofibrils with mostly uniform widths and heights in the same
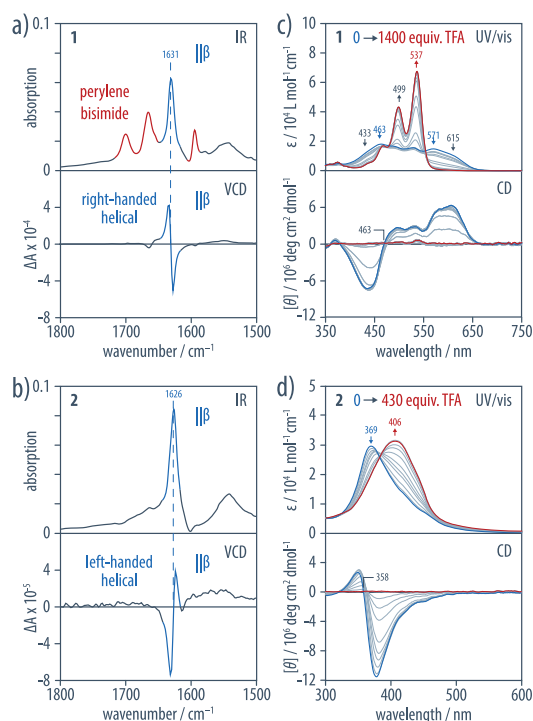
Figure 2. (a,b) IR and VCD spectroscopy of 1 and 2 and (c,d) UV−vis and CD spectroscopy proved the formation of well-defined hydrogen-bonded aggregates in solution as well as the presence of strongly $\pi-\pi$ stacked and helically arranged π-conjugated cores. Thus, the global absorption maximum in the UV−vis spectrum of 1 in the aggregated state (blue curve) was blue-shifted (463 nm) relative to the molecularly dissolved species (537 nm) that was obtained by titration of the solution with an excess of trifluoroacetic acid (red curve). The additional bathochromically shifted absorption band at 569 nm with a shoulder at 615 nm, respectively, suggested the presence of strongly cofacially aggregated but laterally and rotationally displaced perylene bisimide cores. Similarly, the UV−vis absorption of 2 was blue-shifted (369 nm) in the aggregated state (blue curve) as compared to the absorption (406 nm) of a solution after deaggregation with an excess of TFA (red curve). The red-shifted shoulder at around 450 nm can be attributed to a weakly allowed HOMO−LUMO transition. The CD spectrum of 1 in the aggregated state revealed CD bands with a positive Cotton effect for the highest wavelength absorption, suggesting a P-helical environment of the perylene bisimides. Consistently, the VCD spectrum of 1 revealed an intense negative couplet with a zero-crossing located at the wavenumber of maximum absorption of the parallel β-sheet amide I band. Similarly, the CD spectrum of 2 showed a bisignate CD band with a negative Cotton effect, and the VCD spectrum revealed a positive couplet for the β-sheet amide I band, both in agreement with an M-helical arrangement of the molecules.

range (Figure 3b, Supplementary Figure S7). In comparison to 1, however, the AFM imaging proved to be more difficult, and a quantitative evaluation of the dimensions was hampered by the accumulation of nonaggregated material along the edges of (and perhaps underneath) the fibrils. AFM images on mica showed segments with periodic height corrugations, and features in the phase images are suggestive of left-handed twisted tapes, although these features were not quite stable over extended time periods.

A detailed morphological study of the nanofibrils was performed by means of multi-set-point intermittent contact (MUSIC) mode AFM that provides information about the unperturbed topography, as well as hydrophilic/hydrophobic and hard/soft contrast at different amplitude set point ratios A/A_0 in a single measurement run.[42,43] Thus, the topography of nanofibrils from 1 (Figure 3c, "topography") exhibited alternating "bumps" and "grooves" with heights of 3.3 ± 0.2 and 2.0 ± 0.3 nm, respectively, with a periodicity of 79 ± 8 nm.

From the corresponding hydrophilic/hydrophobic contrast image (Figure 3c, "hydrophilicity"), we found the "bumps" to exhibit diagonal features of two light stripes, which may reflect the hydrophobic perylene bisimide core substituted by the more hydrophilic oligopeptides. Moreover, the hard/soft contrast image (Figure 3c, "softness") revealed soft material lining the edges of the nanofibrils as well as a periodic pattern along the nanofibrils, suggesting that the terminally attached hydrophobic poly(isobutylene)s preferentially wetted the substrate. In combination with the rotationally and laterally displaced arrangement of the $\pi-\pi$-stacked perylene bisimide cores proved by UV−vis, CD, and VCD spectroscopy, the MUSIC mode AFM results were, thus, consistent with right-handed helical (curled) tapes (Figure 3e). Furthermore, comparing the available volume per molecule of about 5000 Å³ in the "groove" regions (assuming a packing at 4.6 Å, see below) with the van der Waals volume of 1 of approximately 3900 Å³ suggested that the observed helical nanofibrils comprise a single stack of the perylene bisimides at their core. While this does not preclude that a weak lateral aggregation of the nanofibrils by partial interpenetration of their polymer shells is the origin for the observed ambiguity in periodicities of the height corrugations, we have no indication for any aggregation by β-sheet stacking that would give rise to additional interactions of the chromophores. The nanofibrils are, thus, "single stack" nanowires in the sense that they contain individual $\pi-\pi$ stacks of the chromophores separated from their neighbors.

MUSIC mode AFM investigations on nanofibrils of 2 revealed regular height alternations ("bumps" with a height of 4.6 ± 0.5 nm, "grooves" with a height of 3.5 ± 0.3 nm) with a periodicity of 60 ± 13 nm (Figure 3d). Although in this case, the periodic fine structure could not be resolved from the phase images, neither in the attractive nor the repulsive regimes, the soft polymer was again found to flank the nanofibrils and wet the substrate. Nevertheless, in combination with the evidence for $\pi-\pi$ stacked and rotationally displaced chromophores in an M-helical environment from UV−vis, CD, and VCD spectroscopy, the observed regular height alternations in the case of nanofibrils from 2 may be interpreted as left-handed twisted tapes (Figure 3f).
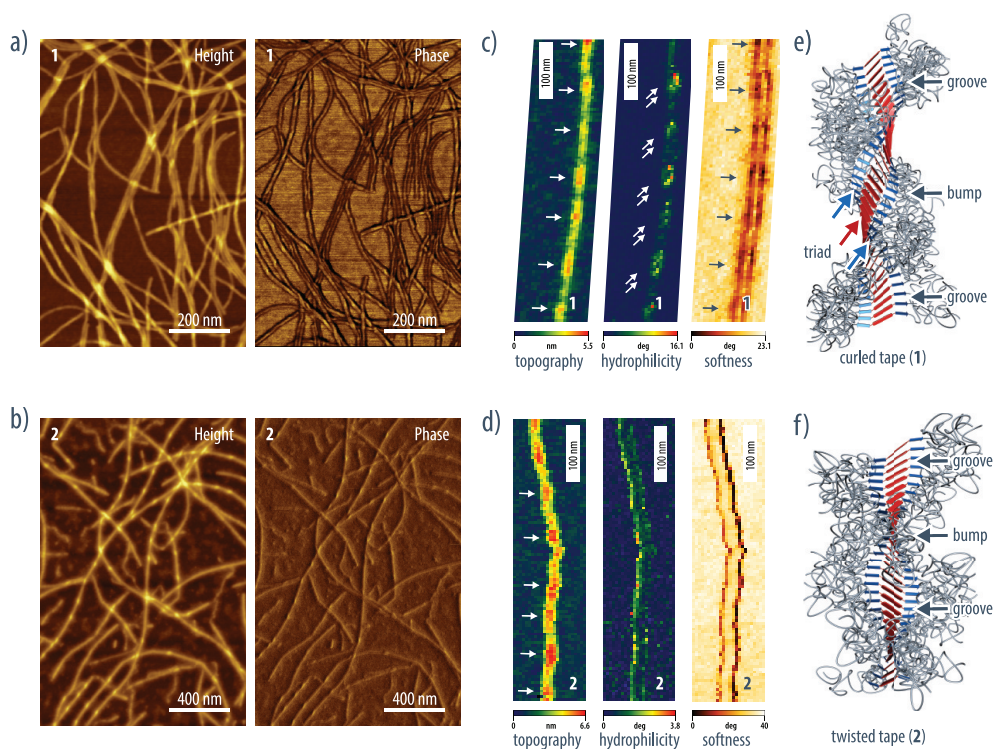
Figure 3. (a,b) Conventional AFM height and phase images of 1 and 2 both showed the formation of many micrometers long single nanofibrils with mostly uniform apparent diameters. (c,d) MUSIC mode AFM images of 1 and 2 showing the unperturbed topography (height at set point $A/A_0 = 1.00$), the hydrophilic/hydrophobic contrast image obtained from the phase image in the attractive regime (at set point $A/A_0 = 0.95$ for 1 and 0.98 for 2; blue = hydrophobic, red = hydrophilic), and the hard/soft contrast image obtained from the phase image in the repulsive regime (at set point $A/A_0 = 0.63$ for 1 and 0.90 for 2; dark = soft, light = hard). In the case of 1, the periodic maxima in the topography image coincided with hydrophilic/ hydrophobic/hydrophilic stripes oriented diagonal to the fiber axis. The hard/soft contrast image showed that the soft polymer segments lined the edges of the fibrils on the surface, but it also revealed periodic features on the fibrils. The topography part of the MUSIC mode AFM images of quaterthiophene 2 revealed periodic corrugations along the fibril axis that were neither resolved in the hydrophilic/hydrophobic nor in the hard/soft contrast images. The latter proved that the soft polymer segments lined the fibril edges and wetted the surface. (e,f) In combination with the spectroscopic results, these findings may be interpreted as right-handed helical (curled) tapes in the case of 1, in which the soft polymers fill the helix grooves. In the case of 2, AFM imaging in combination with spectroscopy suggests the presence of left-handed twisted tapes.

Preparation and Comprehensive Structural Characterization of Microfibers. We fabricated well-defined microfibers by simple solution-spinning of thermally annealed TCE solutions containing nanofibrils of **1** or **2** into MeOH as a nonsolvent (Supplementary Figure S8). The obtained microfibers were constituted from arrays of aligned nanofibrils and allowed us to perform a comprehensive investigation of their hierarchical internal structure down to the molecular level. Thus, the microfibers had lengths of many centimeters and were sufficiently robust to manually place them on substrates or prepare aligned bundles (Figure 4a). Scanning electron microscopy (SEM) proved that the diameters of microfibers of **1** could be tailored by the applied cannula gauge, resulting in narrowly distributed diameters of 18.7 ± 1.6, 10.0 ± 1.6, and 5.7 ± 1.2 μm (Figure 4b, Supplementary Figures S8–S9). At higher magnifications (Figure 4c), it became apparent that the microfibers were hierarchically constituted from highly aligned microfibrils (diameters 1500–2400 nm) and smaller protofibrils (diameters 120–130 nm). AFM imaging on the surface of a microfiber of **1** confirmed

these structural features and, more importantly, revealed that the protofibrils were constituted of highly aligned arrays of densely packed nanofibrils with an apparent diameter of about 6–8 nm (Figure 4d).

Accordingly, maximum birefringence was observed in polarized optical microscopy (POM) under crossed polarizers for single microfibers of **1** when the fiber was placed in diagonal position, and the sample remained black in extinction position (Figure 5a). POM with a 530 nm retardation-plate (slow axis oriented 45° to the polarizers) proved that the refractive indices of the microfibers were higher parallel as opposed to perpendicular to their long axes (Supplementary Figure S10). Moreover, polarized IR microscopy of a single microfiber of **1** (Figure 5b) showed a distinct intensification of the amide A and I bands (3290 and 1624 cm^{-1}) in parallel polarizer orientation and of the amide II absorption (1545 cm^{-1}) in perpendicular polarizer orientation, in agreement with an average orientation of the oligopeptide β-stands perpendicular to the microfiber axis. Thus, POM and polarized IR microscopy clearly indicated that the oligopeptides' N—H and C═O
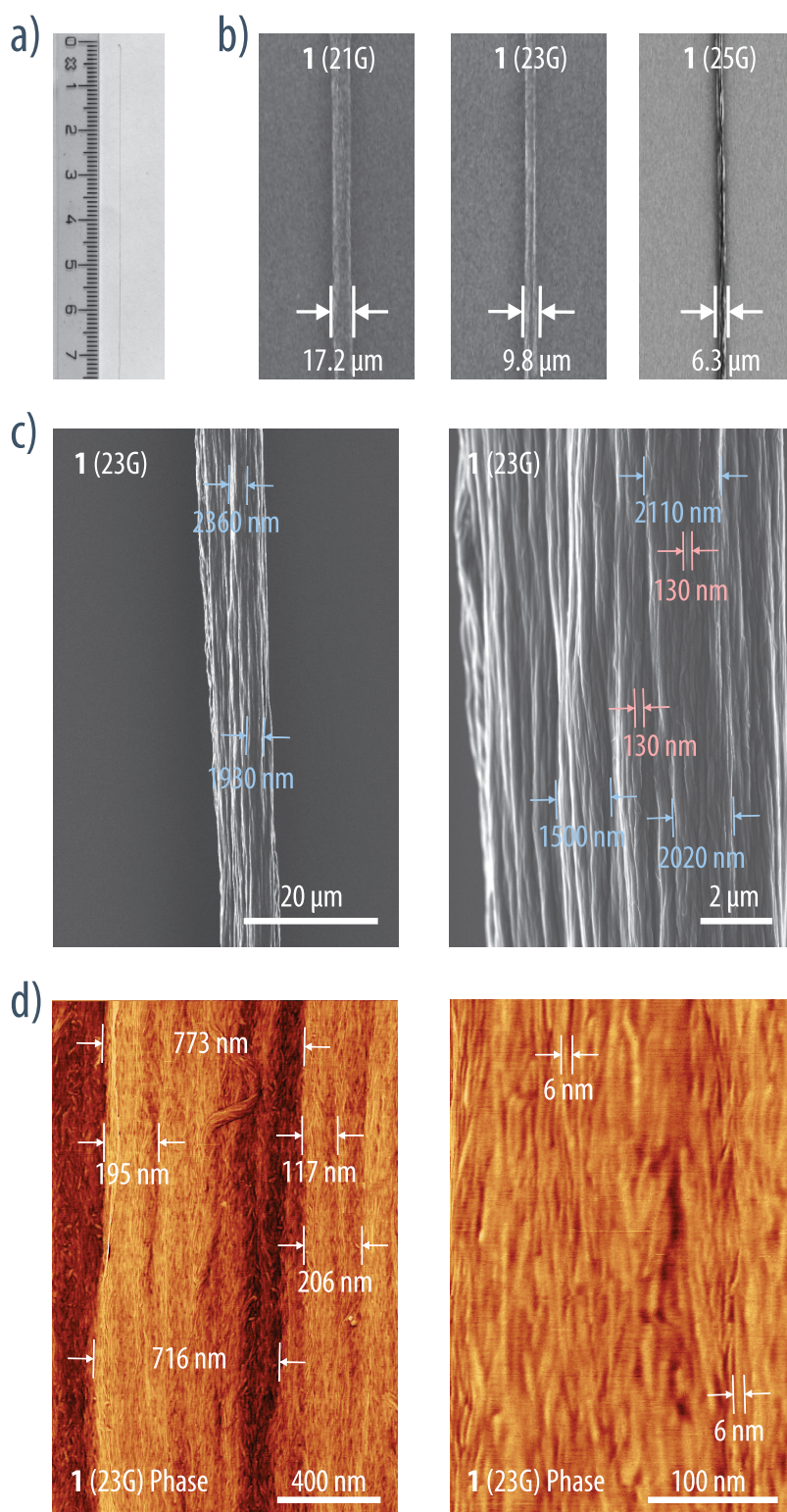
Figure 4. (a) Photograph of a microfiber of 1 obtained by solution-spinning of a nanofibril solution in TCE into MeOH. (b) SEM revealed that the microfibers had diameters controlled by the needle gauge and that (c) the microfibers comprised highly aligned microfibrils (left/middle; diameters 1500–2500 nm) that were constituted of smaller protofibrils (middle/right, diameters 120–130 nm). (d) AFM phase images on the surface of a microfiber of 1 showed that the protofibrils were constituted of highly aligned arrays of the nanofibrils with an apparent diameter of about 6–8 nm.

moieties were oriented parallel to the microfiber axis, consistent with a cross-β-sheet structure in which the oligopeptide β-strands were aligned perpendicular to the microfiber axis, and the β-sheet aggregation determined the fast growth direction of the microfibers and their nanofibrillar constituents.
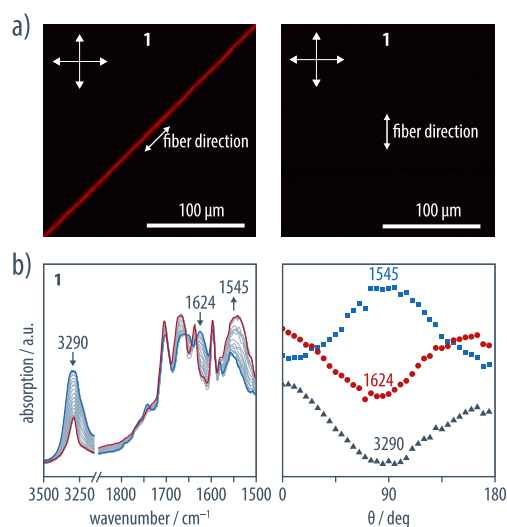
Figure 5. (a) Strong birefringence of single microfibers of **1** was observed under crossed polarizers in diagonal position, while the sample remained dark in extinction position, indicating long-range order within the fibers. **(b)** Amide A, I, and II regions of the polarized IR microscopy spectra of a single microfiber of **1** (left) with the polarizer perpendicular (90°, red) and parallel (0°, blue) to the microfiber showed an intensification of the absorptions at 3290 and 1624 cm^{-1} in parallel orientation and of the 1545 cm^{-1} band in perpendicular orientation. The gray curves represent the intermediate spectra obtained by increasing the angle between the polarizer and the microfiber from 5° to 85° in steps of 5°. Plots of the absorption intensities at 1545 cm^{-1} (blue), 1624 cm^{-1} (red), and 3290 cm^{-1} (gray) *versus* the angle between polarizer and microfiber showed a maximum for the amide II band and a minimum for the amide A band at 90°, as well as a minimum for amide I band at 80°, consistent with an average orientation of the oligopeptide β-stands perpendicular to the microfiber axis, taking into consideration the typical angle of the transition dipole moment of the C=O stretching vibration relative to the C=O bond axis.[41]

Similarly, microfibers of quaterthiophene **2** exhibited controlled and uniform diameters, as proven by SEM imaging (Supplementary Figure S11). However, while the constituting microfibrils appeared to be well aligned in shearing direction, the arrangement of the smaller protofibrils was found to be less ordered in this case. Nevertheless, POM as well as polarized IR microscopy (Supplementary Figures S12, S13) suggested the presence of aligned nanofibrils with an internal structure similar to **1**.

Small-angle X-ray scattering (SAXS) unambiguously proved that microfibers prepared from either **1** or **2** contained highly aligned arrays of the tightly packed nanofibrils. Moreover, wide-angle X-ray scattering (WAXS) allowed us to precisely determine the orientation of each segment of the constituting molecules and revealed that the $\pi-\pi$ stacking of the chromophores was very tight, as a consequence of mutually enhanced $\pi-\pi$ interactions and hydrogen-bonding. Thus, the 2D SAXS patterns and corresponding q-vector plots of manually aligned microfiber bundles of **1** and **2** (Figure 6a, Supplementary Figures S14—S17) revealed single anisotropic reflections at d = 7.24 and 8.24 nm,
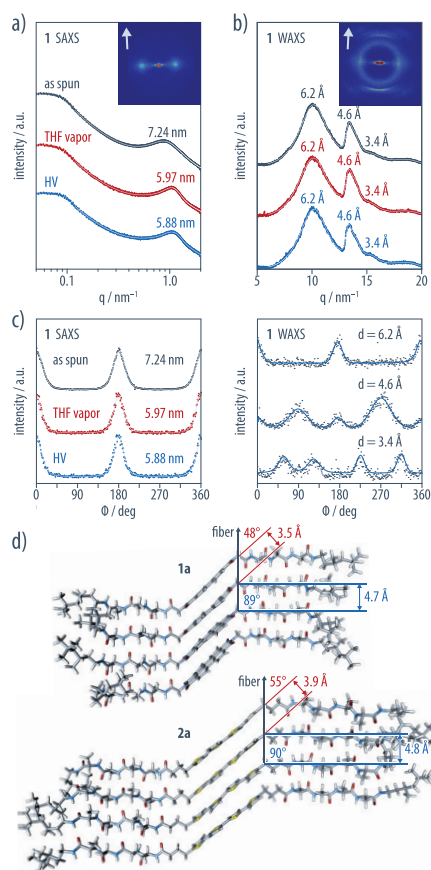
Figure 6. (a,b) The 2D SAXS and WAXS patterns of a non-annealed microfiber bundle of perylene bisimide **1** (gray arrows indicate the microfiber orientation), and q-vector plots of the three differently treated microfiber bundles (gray: nonannealed; red: annealed in THF vapor 7 d; blue: annealed in a high vacuum for 48 h). The SAXS region showed a reflection at a characteristic distances of d = 5.88—7.24 nm (q = 0.87—1.07 nm^{-1}) that can be assigned to the tight packing of the nanofibrils into an aligned array within the microfibers. The observed distance was smaller than the extended length of the molecules and became even smaller upon annealing, indicating that the packing and alignment of the nanofibrils improved. The WAXS reflections were not affected by annealing. The reflections at d = 3.4 Å (q = 18.7—18.8 nm^{-1}), 4.6 Å (q = 13.7—13.8 nm^{-1}), and 6.2 Å (q = 10.1—10.2 nm^{-1}) were assigned to the $\pi-\pi$ stacked conjugated cores, the hydrogen-bonded oligopeptides, and poly(isobutylene), respectively. **(c)** The azimuthal intensity distributions (shown for the sample annealed in high vacuum) revealed two maxima at ϕ = 0° and 180° for the reflections at d = 5.88 nm and d = 6.2 Å; the 4.6 Å reflection showed two maxima at ϕ = 90° and 270° (the two small maxima at 0° and 180° were assigned to residual intensity from the close 6.2 Å reflection), and the 3.4 Å reflection exhibited four maxima at ϕ = 51°, 180° − ϕ, 180° + ϕ, and 360° − ϕ. These results proved that the nanofibrils were aligned parallel to the microfiber axis, with the polymer segments sheared along the same direction. The oligopeptide β-strands were oriented perpendicular to the microfiber axis, and the π-conjugated cores showed a conical distribution with an average inclination angle ϕ relative to the microfiber axis. **(d)** Molecular models of aggregates from **1** and **2** obtained by MD simulations based on starting dodecameric geometries (Supporting Figure S18 and Table S5) with the two innermost oligopeptide carbonyl groups oriented in opposite directions. The observed distances and inclination angles relative to the microfiber axis perfectly matched the experimental values obtained by X-ray scattering.

respectively, with two maxima in the azimuthal distributions at $\phi = 0°$ and $180°$ (Figure 6c). This observation provided unambiguous evidence that the nanofibrils were highly aligned and packed within the microfibers at a distance significantly smaller than the extended molecular length of **1** and **2** of about 14 and 15 nm, respectively, and in excellent agreement with the diameter of about 8 nm observed in the AFM images of **1** on HOPG. This distance further decreased to $d < 6$ nm upon annealing either in THF vapor or in a high vacuum, and the corresponding correlation lengths increased from $\xi = 9.8$ to $16.9-17.4$ nm (Supplementary Figure S15). This finding implies that the poly(isobutylene) segments remained, to some degree, "swollen" by residual solvent; they only completely collapsed upon annealing, which served to tighten and improve the packing and alignment of the nanofibrils parallel to the microfiber axis.

The 2D WAXS patterns and the corresponding q-vector plots of manually aligned microfiber bundles of **1** (Figure 6b, Supplementary Figure S14–S16) showed two anisotropic reflections at characteristic distances of $d_{\pi-\pi} = 3.4$ Å and $d_\beta = 4.6$ Å, as well as a broad third reflection at $d_{PIB} = 6.2$ Å that can be assigned to the $\pi-\pi$ stacking of the perylene bisimide cores, the β-sheet-like aggregation of the oligopeptides, and the packing of poly(isobutylene)s in a (short-range) 8_3-helical conformation,[44,45] respectively. It is worth noting that the observed hydrogen-bonding distance is significantly shorter than the 4.8 Å typically observed in natural β-sheets, reflecting the stronger N—H···O=C hydrogen-bonding in a hydrophobic environment. At the same time, a $\pi-\pi$ stacking as tight as 3.4 Å is significantly smaller than the previously reported values of $3.55-3.75$ Å for self-assembled systems determined by X-ray diffraction[28,30] and almost matches the distance of 3.35 Å observed in some perylene bisimide single crystals[46] or for the interlayer distance in graphite. Moreover, the azimuthal intensity distributions (Figure 6c) of the microfiber bundles in comparison to randomly oriented samples of **1** proved that the 4.6 Å reflection exhibited maxima at $\phi = 90°$ and $270°$, indicative of an orientation of the oligopeptide β-strands perpendicular to the microfiber axis and consistent with the POM and polarized IR microscopy results. By contrast, the 3.4 Å reflection showed four maxima corresponding to a conical distribution of the perylene bisimides with an average inclination of $\phi = 48-51°$ relative to the fiber axis and a high degree of internal order, perfectly fulfilling the trigonometric relation $\sin \phi = d_{\pi-\pi}/d_\beta$. This observation emphasizes the importance of including some conformational flexibility between the oligopeptides and the π-conjugated segments in order to decouple the respective geometric requirements of hydrogen-bonding and $\pi-\pi$ stacking, that is, the different spacing and the lateral offset of the

π-conjugated cores required for constructive π-overlap. In this way, the two different supramolecular interactions do not impede but even synergistically enhance each other so that the strong hydrogen-bonding in a hydrophobic environment induces a tight $\pi-\pi$ stacking inside the nanofibrils.

Similar to **1**, WAXS of a manually aligned microfiber bundle of quaterthiophene **2** showed three anisotropic reflections characteristic for the $\pi-\pi$ stacking, hydrogen-bonding and poly(isobutylene) 8_3-helices at $d_{\pi-\pi} = 3.2$ Å, $d_\beta = 4.5$ Å, and $d_{PIB} = 6.0$ Å, respectively (Supplementary Figure S17). In contrast to **1**, however, the spacing of the broad and poorly resolved $d_{\pi-\pi}$ reflection must be interpreted with caution, and no azimuthal intensity distribution could be reliably determined for it, indicating a higher degree of disorder and conformational dynamics in the case of the quaterthiophene derivatives. Nevertheless, it should be noted that the strong exciton coupling of about 0.6 eV observed in the UV–vis spectra of **2** (Figure 2d) is consistent with a $\pi-\pi$ stacking of the quaterthiophene cores at a smaller spacing than, for instance, the interlayer distance of 3.8 Å typically observed in regioregular poly(3-hexylthiophene) (P3HT) and comparable to the 3.4 Å recently reported for certain low molecular weight P3HT oligomers.[47]

In summary, SAXS and WAXS experiments demonstrated that the nanofibrils were formed as a result of combined hydrogen-bonding and $\pi-\pi$ interactions, giving rise to tight $\pi-\pi$ stacking and a conical distribution of the chromophores, consistent with their helical supramolecular arrangement. Moreover, considering that the maxima of the azimuthal intensity distributions of the d_{PIB} WAXS reflection at $\phi = 0°$ and $180°$ implied that poly(isobutylene) segments had been sheared along the microfiber axis during the spinning process, one may confer that they filled the "voids" (the helix grooves of the tapes) at the nanofibrils' core in their collapsed state, as it had also been concluded from the MUSIC mode AFM images (Figure 3c). As a result, the central stack of π-conjugated cores is periodically covered with only a shallow shell (<1 nm) of the insulating poly(isobutylene)s and, hence, less shielded than the molecular structures of **1** and **2** appear to imply, which will be relevant in the context of using such nanofibrils and microfibers in organic electronic devices.

Molecular Dynamics Simulations. In order to obtain an atomistic understanding of the supramolecular aggregates and their structural dynamics, we performed molecular dynamics (MD) simulations at the classical molecular mechanics level for dodecameric aggregates of **1** and **2**, with their polymer termini replaced by simple alkyl groups (Figure 6d, Supplementary Figure S18, Table S5). The starting geometries were constructed on the basis of regular stacks of conformationally extended molecules with inclination angles

relative to the microfiber axis of 90° for both the oligopeptide and the π-conjugated segments, and considering two possible molecular conformations and supramolecular arrangements in each case. While one set of models (**1b** and **2b** in Supplementary Figure S18) could be discarded by comparison to the experimental results, equilibration (25 ns) and simulation (15 ns) of **1a** resulted in a packing of the oligopeptides at a distance of 4.8 ± 0.1 Å, a $\pi-\pi$ stacking distance between the perylene bisimide cores of 3.5 ± 0.1 Å, with inclination angles relative to the microfiber axis of 89 ± 2° and 48 ± 2°, respectively, in excellent agreement with the X-ray data. Similarly, MD simulations of **2a** furnished an oligopeptide packing at a distance of 4.8 ± 0.1 Å (inclination 90° ± 3°) and a $\pi-\pi$-stacking distance of 3.9 ± 0.2 Å (inclination 55° ± 4°). Notably, the aggregates **2a** were more "flexible" compared to **1a**. In agreement with the higher disorder observed in the X-ray analysis of **2**, they exhibited overall significantly higher structural and conformational dynamics and disorder, presumably due to weaker $\pi-\pi$ stacking. While the simulations yielded a "curled" aggregate for **1** and a twisted stack for **2**, in excellent agreement with the AFM results, the rotational displacement angles showed large standard deviations, and achieving the "correct" (experimentally observed) handedness is apparently beyond the ability of current force field parameters. Theoretical UV–vis spectra for a single perylene bisimide core as well as a stack of four perylene bisimides extracted from average geometries of an MD trajectory of **1** were then obtained by density functional theory (DFT) computations at the ωB97X-D[48]/def2-SVP[49] level (Supplementary Figure S19). The disappearance of the monomer peak combined with the appearance of one hypsochromically and two bathochromically shifted absorption bands in the aggregates are in excellent qualitative agreement with our experimental findings, lending further credibility to the proposed models of the aggregates.

CONCLUSIONS

We presented a versatile supramolecular strategy to prepare well-defined one-dimensional nanofibrils comprising single stacks of either electron-poor perylene bisimides or electron-rich quaterthiophenes at their core. From these nanofibrils, we prepared microfibers that exhibited hierarchical structure formation with a remarkably high degree of internal order, ranging from the supramolecular level (hydrogen-bonding, $\pi-\pi$ stacking) over nanostructure formation (arrays of aligned and densely packed nanofibrils) up to the microscopic length scale (tailored diameter and uniform morphology). This achievement has, in turn, allowed us to rigorously perform structure characterization on all levels of the structural hierarchy with molecular level precision and, thus, obtain a better understanding of how all of these levels are intimately coupled and interrelated. Our results indicate that the molecular chirality expressed as supramolecular helicity serves to suppress lateral aggregation of the chromophores. Moreover, the inclusion of conformational flexibility between the oligopeptides and the π-conjugated segments decouples the geometric requirements of hydrogen-bonding and $\pi-\pi$ stacking so that these two supramolecular interactions even synergistically enhance one another. As a result, the strong hydrogen-bonding in a hydrophobic environment induces a remarkably tight $\pi-\pi$ stacking inside the nanofibrils, which may be regarded as the structural basis for their efficient charge generation and transport properties. Hence, because of their well-established internal structure and the fact that their self-organization is agnostic to the electronic nature of the included π-conjugated segment, the obtained nanofibrils and microfibers are suitable model systems for the investigation of one-dimensional charge transport along well-defined stacks of p-type or n-type organic semiconductors that may also serve as charge percolation paths in future nanoelectronic devices.

METHODS

Materials. Compounds **1** and **2** were synthesized analogously to published procedures[34] and characterized by NMR spectroscopy as well as mass spectrometry. Spectroscopy grade solvents were used for all spectroscopic investigations.

Thermal Annealing of Nanofibril Solutions. Thermal annealing of organic solutions containing nanofibrils of **1** and **2** turned out to be crucial for obtaining well-defined nanofibrils with a high aspect-ratio (Supplementary Figure S6, S7). For this purpose, 10 mL of solution of **1** or **2** in tetrachloroethane (TCE) ($c = 1 \times 10^{-3}$ mol/L) was placed into a 25 mL Schlenk-tube equipped with a magnetic stir bar and a screw cap. The tube was sealed, degassed in three freeze–pump–thaw cycles, and then flushed with argon. The solution was vigorously stirred (400 rpm) at an oil bath temperature of 180 °C (that is, significantly above the boiling point of TCE) for 4 h. The stirring speed was then reduced to 200 rpm, and the solution was slowly allowed to cool (4 h at 165 °C, 16 h at 150 °C, 4 h at 135 °C, 4 h at 120 °C, 16 h

at 100 °C, 4 h at 80 °C, 4 h at 60 °C). The heating plate was finally switched off, and the solution was allowed to cool to room temperature while continuing to stir for another 24 h. The thus obtained solutions were used for spectroscopy, AFM imaging, and solution-spinning of microfibers.

Solution-Spinning of Microfibers. Microfibers were obtained by injection of an annealed TCE solution of **1** or **2** through a syringe needle dipped into a vial or glass cylinder containing MeOH (Supplementary Figure S8). The plunger was gently pushed at the beginning of the spinning process to bring the TCE solution in the needle into contact with the MeOH, which triggered a continuous flow of TCE solution out of the needle. Once the microfiber had reached the desired length, the needle tip was simply moved out of the MeOH to stop the process, and the microfiber sticking to the needle could easily be recovered and manipulated. With this procedure, we obtained well-defined microfibers with lengths of up to several centimeters. Furthermore, the microfibers' diameter could be controlled by varying the needles' gauge. Thus, microfibers with diameters of

18.7 ± 1.6, 10.0 ± 1.6, and 5.7 ± 1.2 μm were obtained for 21G, 23G, and 25G needles that had 495, 318, and 241 μm internal diameters, respectively.

Atomic Force Microscopy Imaging. Thermally annealed solutions of **1** and **2** in TCE were diluted to a concentration of 5×10^{-5} mol/L and then drop-cast on mica (in case of sample **1** also on HOPG) and gently dried in air flow. The samples were analyzed in tapping mode using a Nanoscope 8 (Bruker, USA) instrument at room temperature in air. Cantilevers with a resonance frequency on average of $f_0 = 150$ kHz and $k = 5$ N/m were used. Scan rates between 0.5 and 2 Hz were applied; the image resolution was 512 × 512 pixels. The MUSIC-mode AFM measurements were performed under ambient conditions as described before.[42,43] SiO$_x$ substrates were first cleaned with an ethanol–toluene mixture and then with a CO$_2$ snow-jet. Standard silicon probes (Pointprobe NCH, NanoWorld AG, Neuchâtel, Switzerland) and a NanoWizard II AFM (JPK Instruments AG, Berlin, Germany) was used. The resonance frequency of the cantilever was $f_0 = 386.366$ kHz, the quality factor was $Q = 360$, and the force constant was determined to $k = 17.3$ N/m.[42,43] An array of 25 × 100 amplitude-phase-distance (APD) curves ($A_0 = 24$ nm, $A_{min} = 15$ nm) was measured on an area of 125 nm by 500 nm. From this data the MUSIC mode AFM height and phase images were reconstructed for different amplitude set points as described before.[42,43]

SAXS and WAXS Measurements. Aligned bundles of microfibers of **1** and **2** were prepared after solution-spinning by guiding the microfiber end stuck to the cannula tip to the other end of the microfiber, resulting in a loop that entwined when pulling the cannula out of the MeOH. This procedure was repeated two more times in order to obtain small bundles of eight microfibers. Following the same technique, 25 of these bundles were then aligned in MeOH in order to obtain an approximately 400 μm thick bundle containing 200 aligned microfibers (Supplementary Figure S14). Nonaligned microfiber samples were obtained by simply coiling several single microfibers into a small lump of material. Completely nonaligned samples were prepared by precipitation of a thermally annealed TCE solution containing nanofibrils of **1** or **2** into MeOH. Annealing of the microfiber samples was achieved by either exposing them to THF vapor for 7 d, or by drying at reduced pressure (1×10^{-3} mbar) for 48 h. SAXS and WAXS experiments were performed on these samples using a Rigaku MicroMax-002+ microfocused beam (4 kW, 45 kV, 0.88 mA) in order to obtain direct information on the SAXS and WAXS reflections. The Cu Kα radiation ($\lambda_{CuK\alpha} = 1.5418$ Å) was collimated by three pinhole (0.4, 0.3, and 0.8 mm) collimators. The scattered X-ray intensity was detected by a Fuji Film BASMS 2025 imaging plate system (15.2 × 15.2 cm^2, 50 μm resolution) and a two-dimensional Triton-200 X-ray detector (20 cm diameter, 200 mm resolution), for WAXS and SAXS regions, respectively. An effective scattering vector range of 0.05 nm$^{-1} < q < 25$ nm^{-1} was obtained, where q is the scattering wave vector defined as $q = 4\pi \sin \theta / \lambda_{CuK\alpha}$, with a scattering angle of 2θ.

Conflict of Interest: The authors declare no competing financial interest.

Supporting Information Available: Supplementary Figures S1–S19 and Supplementary Tables S1–S5, including UV–vis, CD, and IR spectra, AFM, SEM, and POM images and their analysis, polarized IR microscopy spectra, 2D SAXS and WAXS patterns as well the corresponding q-vector plots and azimuthal intensity distributions. Details about IR, UV–vis, CD, and VCD spectroscopy, IR microscopy, POM, SLS, SEM, computational details, results of MD simulations as PDB files, as well as graphical representations, analytical data for novel compounds, and an appendix of NMR and mass spectra thereof. This material is available free of charge *via* the Internet at http://pubs.acs.org.

REFERENCES AND NOTES

1. Zhao, Y. S.; Wu, J.; Huang, J. Vertical Organic Nanowire Arrays: Controlled Synthesis and Chemical Sensors. *J. Am. Chem. Soc.* **2009**, *131*, 3158–3159.

2. Che, Y.; Yang, X.; Loser, S.; Zang, L. Expedient Vapor Probing of Organic Amines Using Fluorescent Nanofibers Fabricated from an n-Type Organic Semiconductor. *Nano Lett.* **2008**, *8*, 2219–2223.

3. Che, Y.; Gross, D. E.; Huang, H.; Yang, D.; Yang, X.; Discekici, E.; Xue, Z.; Zhao, H.; Moore, J. S.; Zang, L. Diffusion-Controlled Detection of Trinitrotoluene: Interior Nanoporous Structure and Low Highest Occupied Molecular Orbital Level of Building Blocks Enhance Selectivity and Sensitivity. *J. Am. Chem. Soc.* **2012**, *134*, 4978–4982.

4. Wicklein, A.; Ghosh, S.; Sommer, M.; Würthner, F.; Thelakkat, M. Self-Assembly of Semiconductor Organogelator Nanowires for Photoinduced Charge Separation. *ACS Nano* **2009**, *3*, 1107–1114.

5. Xin, H.; Kim, F. S.; Jenekhe, S. A. Highly Efficient Solar Cells Based on Poly(3-butylthiophene) Nanowires. *J. Am. Chem. Soc.* **2008**, *130*, 5424–5425.

6. Schmidt-Mende, L.; Fechtenkötter, A.; Müllen, K.; Moons, E.; Friend, R. H.; MacKenzie, J. D. Self-Organized Discotic Liquid Crystals for High-Efficiency Organic Photovoltaics. *Science* **2001**, *293*, 1119–1122.

7. Yamamoto, Y.; Fukushima, T.; Suna, Y.; Ishii, N.; Saeki, A.; Seki, S.; Tagawa, S.; Taniguchi, M.; Kawai, T.; Aida, T. Photoconductive Coaxial Nanotubes of Molecularly Connected Electron Donor and Acceptor Layers. *Science* **2006**, *314*, 1761–1764.

8. Briseno, A. L.; Mannsfeld, S. C. B.; Jenekhe, S. A.; Bao, Z.; Xia, Y. Introducing Organic Nanowire Transistors. *Mater. Today* **2008**, *11*, 38–47.

9. Xiao, S.; Tang, J.; Beetz, T.; Guo, X.; Tremblay, N.; Siegrist, T.; Zhu, Y.; Steigerwald, M.; Nuckolls, C. Transferring Self-Assembled, Nanoscale Cables into Electrical Devices. *J. Am. Chem. Soc.* **2006**, *128*, 10700–10701.

10. Grozema, F. C.; Siebbeles, L. D. A. Mechanism of Charge Transport in Self-Organizing Organic Materials. *Int. Rev. Phys. Chem.* **2008**, *27*, 87–138.

11. Aleshin, A. N.; Lee, H. J.; Park, Y. W.; Akagi, K. One-Dimensional Transport in Polymer Nanofibers. *Phys. Rev. Lett.* **2004**, *93*, 196601.

12. Kim, F. S.; Ren, G.; Jenekhe, S. A. One-Dimensional Nanostructures of π-Conjugated Molecular Systems: Assembly, Properties, and Applications from Photovoltaics, Sensors, and Nanophotonics to Nanoelectronics. *Chem. Mater.* **2010**, *23*, 682–732.

13. Faramarzi, V.; Niess, F.; Moulin, E.; Maaloum, M.; Dayen, J. F.; Beaufrand, J. B.; Zanettini, S.; Doudin, B.; Giuseppone, N. Light-Triggered Self-Construction of Supramolecular Organic Nanowires as Metallic Interconnects. *Nat. Chem.* **2012**, *4*, 485–490.

14. Kim, D. H.; Lee, D. Y.; Lee, H. S.; Lee, W. H.; Kim, Y. H.; Han, J. I.; Cho, K. High-Mobility Organic Transistors Based on Single-Crystalline Microribbons of Triisopropylsilylethynyl Pentacene *via* Solution-Phase Self-Assembly. *Adv. Mater.* **2007**, *19*, 678–682.

15. Briseno, A. L.; Mannsfeld, S. C. B.; Lu, X.; Xiong, Y.; Jenekhe, S. A.; Bao, Z.; Xia, Y. Fabrication of Field-Effect Transistors from Hexathiapentacene Single-Crystal Nanowires. *Nano Lett.* **2007**, *7*, 668–675.

16. Ahmed, E.; Earmme, T.; Ren, G.; Jenekhe, S. A. Novel n-Type Conjugated Ladder Heteroarenes: Synthesis, Self-Assembly of Nanowires, Electron Transport, and Electroluminescence of Bisindenoanthrazolines. *Chem. Mater.* **2010**, *22*, 5786–5796.

17. Balakrishnan, K.; Datar, A.; Oitker, R.; Chen, H.; Zuo, J.; Zang, L. Nanobelt Self-Assembly from an Organic n-Type

Semiconductor: Propoxyethyl-PTCDI. *J. Am. Chem. Soc.* **2005**, *127*, 10496–10497.

18. Ajayaghosh, A.; George, S. J. First Phenylenevinylene Based Organogels: Self-Assembled Nanostructures *via* Cooperative Hydrogen Bonding and π-Stacking. *J. Am. Chem. Soc.* **2001**, *123*, 5148–5149.

19. Schwab, A. D.; Smith, D. E.; Bond-Watts, B.; Johnston, D. E.; Hone, J.; Johnson, A. T.; de Paula, J. C.; Smith, W. F. Photoconductivity of Self-Assembled Porphyrin Nanorods. *Nano Lett.* **2004**, *4*, 1261–1265.

20. Shao, H.; Parquette, J. R. A π-Conjugated Hydrogel Based on an Fmoc-Dipeptide Naphthalene Diimide Semiconductor. *Chem. Commun.* **2010**, *46*, 4285–4287.

21. Sun, Y.; Tan, L.; Jiang, S.; Qian, H.; Wang, Z.; Yan, D.; Di, C.; Wang, Y.; Wu, W.; Yu, G.; et al. High-Performance Transistor Based on Individual Single-Crystalline Micrometer Wire of Perylo[1,12-b,c,d]thiophene. *J. Am. Chem. Soc.* **2007**, *129*, 1882–1883.

22. Hong, D.-J.; Lee, E.; Lee, M. Nanofibers from Self-Assembly of an Aromatic Facial Amphiphile with Oligo(ethylene oxide) Dendrons. *Chem. Commun.* **2007**, 1801–1803.

23. Lee, C. C.; Grenier, C.; Meijer, E. W.; Schenning, A. P. H. J. Preparation and Characterization of Helical Self-Assembled Nanofibers. *Chem. Soc. Rev.* **2009**, *38*, 671–683.

24. Balakrishnan, K.; Datar, A.; Zhang, W.; Yang, X.; Naddo, T.; Huang, J.; Zuo, J.; Yen, M.; Moore, J. S.; Zang, L. Nanofibril Self-Assembly of an Arylene Ethynylene Macrocycle. *J. Am. Chem. Soc.* **2006**, *128*, 6576–6577.

25. Hernando, J.; de Witte, P. A. J.; van Dijk, E. M. H. P.; Korterik, J.; Nolte, R. J. M.; Rowan, A. E.; García-Parajó, M. F.; van Hulst, N. F. Investigation of Perylene Photonic Wires by Combined Single-Molecule Fluorescence and Atomic Force Microscopy. *Angew. Chem., Int. Ed.* **2004**, *43*, 4045–4049.

26. Würthner, F.; Bauer, C.; Stepanenko, V.; Yagai, S. A Black Perylene Bisimide Super Gelator with an Unexpected J-Type Absorption Band. *Adv. Mater.* **2008**, *20*, 1695–1698.

27. Vadehra, G. S.; Wall, B. D.; Diegelmann, S. R.; Tovar, J. D. On-Resin Dimerization Incorporates a Diverse Array of pi-Conjugated Functionality within Aqueous Self-Assembling Peptide Backbones. *Chem. Commun.* **2010**, *46*, 3947–3949.

28. Yagai, S.; Seki, T.; Murayama, H.; Wakikawa, Y.; Ikoma, T.; Kikkawa, Y.; Karatsu, T.; Kitamura, A.; Honsho, Y.; Seki, S. Structural and Electronic Properties of Extremely Long Perylene Bisimide Nanofibers Formed through a Stoichiometrically Mismatched, Hydrogen-Bonded Complexation. *Small* **2010**, *6*, 2731–2740.

29. Wall, B. D.; Diegelmann, S. R.; Zhang, S.; Dawidczyk, T. J.; Wilson, W. L.; Katz, H. E.; Mao, H.-Q.; Tovar, J. D. Aligned Macroscopic Domains of Optoelectronic Nanostructures Prepared *via* Shear-Flow Assembly of Peptide Hydrogels. *Adv. Mater.* **2011**, *23*, 5009–5014.

30. Marcon, V.; Breiby, D. W.; Pisula, W.; Dahl, J.; Kirkpatrick, J.; Patwardhan, S.; Grozema, F.; Andrienko, D. Understanding Structure-Mobility Relations for Perylene Tetracarboxydiimide Derivatives. *J. Am. Chem. Soc.* **2009**, *131*, 11426–11432.

31. Pisula, W.; Tomovic, Z.; Simpson, C.; Kastler, M.; Pakula, T.; Müllen, K. Relationship between Core Size, Side Chain Length, and the Supramolecular Organization of Polycyclic Aromatic Hydrocarbons. *Chem. Mater.* **2005**, *17*, 4296–4303.

32. Brédas, J. L.; Calbert, J. P.; da Silva Filho, D. A.; Cornil, J. Organic Semiconductors: A Theoretical Characterization of the Basic Parameters Governing Charge Transport. *Proc. Natl. Acad. Sci. U. S. A.* **2002**, *99*, 5804–5809.

33. Henson, Z. B.; Müllen, K.; Bazan, G. C. Design Strategies for Organic Semiconductors Beyond the Molecular Formula. *Nat. Chem.* **2012**, *4*, 699–704.

34. Tian, L.; Szilluweit, R.; Marty, R.; Bertschi, L.; Zerson, M.; Spitzner, E.-C.; Magerle, R.; Frauenrath, H. Development of a Robust Supramolecular Method to Prepare Well-Defined Nanofibrils from Conjugated Molecules. *Chem. Sci.* **2012**, *3*, 1512–1521.

35. SLS analysis of solutions of **1** failed because of intense absorption/fluorescence.

36. Chen, Z.; Stepanenko, V.; Dehm, V.; Prins, P.; Siebbeles, L. D. A.; Seibt, J.; Marquetand, P.; Engel, V.; Würthner, F. Photoluminescence and Conductivity of Self-Assembled $\pi-\pi$ Stacks of Perylene Bisimide Dyes. *Chem.—Eur. J.* **2007**, *13*, 436–449.

37. Thalacker, C.; Würthner, F. Chiral Perylene Bisimide−Melamine Assemblies: Hydrogen Bond-Directed Growth of Helically Stacked Dyes with Chiroptical Properties. *Adv. Funct. Mater.* **2002**, *12*, 209–218.

38. Dehm, V.; Chen, Z.; Baumeister, U.; Prins, P.; Siebbeles, L. D. A.; Würthner, F. Helical Growth of Semiconducting Columnar Dye Assemblies Based on Chiral Perylene Bisimides. *Org. Lett.* **2007**, *9*, 1085–1088.

39. Hu, J.; Wenfeng, K.; Deng, K.; Zou, W.; Huang, Y.; Wei, Z.; Faul, C. F. J. Self-Assembled Sugar-Substituted Perylene Diimide Nanostructures with Homochirality and High Gas Sensitivity. *Adv. Funct. Mater.* **2012**, *22*, 4149–4158.

40. Kawano, S.-I.; Fujita, N.; Shinkai, S. Quater-, Quinque-, and Sexithiophene Organogelators: Unique Thermochromism and Heating-Free Sol-Gel Phase Transition. *Chem.—Eur. J.* **2005**, *11*, 4735–4742.

41. Measey, T. J.; Schweitzer-Stenner, R. Vibrational Circular Dichroism as a Probe of Fibrillogenesis: The Origin of the Anomalous Intensity Enhancement of Amyloid-like Fibrils. *J. Am. Chem. Soc.* **2011**, *133*, 1066–1076.

42. Spitzner, E.-C.; Riesch, C.; Szilluweit, R.; Tian, L.; Frauenrath, H.; Magerle, R. Multi-Set Point Intermittent Contact (MUSIC) Mode Atomic Force Microscopy of Oligothiophene Fibrils. *ACS Macro Lett.* **2012**, *1*, 380–383.

43. Spitzner, E.-C.; Riesch, C.; Magerle, R. Subsurface Imaging of Soft Polymeric Materials with Nanoscale Resolution. *ACS Nano* **2011**, *5*, 315–320.

44. Tanaka, T.; Chatani, Y.; Tadokoro, H. Crystal Structure of Polyisobutylene. *J. Polym. Sci., Polym. Phys. Ed.* **1974**, *12*, 515–531.

45. Suter, U. W.; Saiz, E.; Flory, P. J. Conformational Characteristics of Polyisobutylene. *Macromolecules* **1983**, *16*, 1317–1328.

46. Zhao, H. M.; Pfister, J.; Settels, V.; Renz, M.; Kaupp, M.; Dehm, V. C.; Würthner, F.; Fink, R. F.; Engels, B. Understanding Ground- and Excited-State Properties of Perylene Tetracarboxylic Acid Bisimide Crystals by Means of Quantum Chemical Computations. *J. Am. Chem. Soc.* **2009**, *131*, 15660–15668.

47. Kayunkid, N.; Uttiya, S.; Brinkmann, M. Structural Model of Regioregular Poly(3-hexylthiophene) Obtained by Electron Diffraction Analysis. *Macromolecules* **2010**, *43*, 4961–4967.

48. Chai, J.-D.; Head-Gordon, M. Long-Range Corrected Hybrid Density Functionals With Damped Atom-Atom Dispersion Corrections. *Phys. Chem. Chem. Phys.* **2008**, *10*, 6615–6620.

49. Weigend, F.; Ahlrichs, R. Balanced Basis Sets of Split Valence, Triple Zeta Valence and Quadruple Zeta Valence Quality for H to Rn: Design and Assessment of Accuracy. *Phys. Chem. Chem. Phys.* **2005**, *7*, 3297–3305.